Biol Cybern (2013) 107:653–667
DOI 10.1007/s00422-013-0565-3

OPINION PAPER

Biological Cybernetics

Computational model of motor learning and perceptual change

Satoshi Ito · Mohammad Darainy · Minoru Sasaki · David J. Ostry

Received: 14 March 2012 / Accepted: 13 August 2013 / Published online: 30 August 2013

Abstract Motor learning in the context of arm reaching movements has been frequently investigated using the paradigm of force-field learning. It has been recently shown that changes to somatosensory perception are likewise associated with motor learning. Changes in perceptual function may be the reason that when the perturbation is removed following motor learning, the hand trajectory does not return to a straight line path even after several dozen trials. To explain the computational mechanisms that produce these characteristics, we propose a motor control and learning scheme using a simplified two-link system in the horizontal plane: We represent learning as the adjustment of desired joint-angular trajectories so as to achieve the reference trajectory of the hand. The convergence of the actual hand movement to the reference trajectory is proved by using a Lyapunov-like lemma, and the result is confirmed using computer simulations. The model assumes that changes in the desired hand trajectory influence the perception of hand position and this in turn affects movement control. Our computer simulations support the idea that perceptual change may come as a result of adjustments to movement planning with motor learning.

S. Ito (✉) · M. Sasaki
Gifu University, Gifu, Japan
e-mail: satoshi@gifu-u.ac.jp

S. Ito · M. Darainy · D. J. Ostry
McGill University, Montreal, Canada

M. Darainy
Shahed University, Tehran, Iran

D. J. Ostry
Haskins Laboratories, New Haven,
CT, USA

Keywords Reaching movement · Motor learning · Somatosensory perceptual change · Computational model · Force field

1 Introduction

Motor learning contributes to the important ability to behave adaptively in various situations. Motor learning has been modeled in various frameworks such as artificial neural networks, optimization, adaptive control, and reinforcement learning among others (Aström and Wittenmark 1989; Sutton and Barto 1998; Nguyen-Tuong and Peters 2011). However, the behaviors of biological system are complex, hierarchal, yet flexible from the viewpoint of control and learning. Thus, it is difficult to integrate the variety of phenomena that characterize learning in a single framework and to advance models that are applicable to the considerable variety of situations entailed in learning. As a result and understandably, recent models of learning are frequently restricted to the explanation of specific cases.

Among the large repertoire of human movements, reaching movements of the arm have been particularly well studied. Thanks to the development of the sophisticated measurement techniques, reaching movements and learning have been investigated in the context of trajectory generation (Flash and Hogan 1985; Uno et al. 1989; Todorov and Jordan 1998; Berret et al. 2011), impedance or stiffness control (Mussa-Ivaldi et al. 1985; Katayama and Kawato 1993; Tsuji et al. 1995; Darainy et al. 2009), and overall movement control strategies (Flash 1987; Wolpert et al. 1995; Gomi and Kawato 1996; Gribble et al. 1998; Kistemaker et al. 2007). A variety of learning models have been proposed for arm reaching movement: Some studies have postulated an inverse dynamics model of the arm to compute the torques that are needed

to achieve desired movement trajectories. Such an inverse model could be acquired using an artificial neural network approach (Miyamoto et al. 1988; Huang et al. 2008) or by estimating parameters of the dynamical system (Slotine and Li 1987; Galicki 2007). Another approach has been to consider learning in the context of patterns of muscle activity where issues of redundancy and limb impedance come into play, and necessitate the introduction of predictive forward models to deal with time delays (Bhushan and Shadmehr 1999; Kambara et al. 2009; Tee et al. 2010). The calculation of desired trajectory has also been used for modeling motor learning (Massone and Bizzi 1989), especially in the context of environmental uncertainty such as in force-field conditions (Shadmehr and Mussa-Ivaldi 1994). Finally, optimal control based on the linear-quadratic-Gaussian method (Todorov and Jordan 2002; Izawa et al. 2008; Mitrovic et al. 2011) has been shown to produce simulated hand paths similar to those in empirical studies without calculating a predefined reference trajectory on the assumption that, in noisy environments such as biological systems, smoother trajectories reduce end point variance.

The present paper proposes a learning model for arm reaching movement. A novel feature of our model is that it contains both motor learning and its effect on somatosensory perception. As in Shadmehr and Mussa-Ivaldi (1994), our motor learning model serves to account for adaptation under force-field conditions but it is distinguished by having an online trial-by-trial adaptation scheme in which stability is ensured given some basic assumptions (see Sect. 2.2). The model consists of a feedforward controller that compensates for the dynamics of the multi-joint arm, a feedback controller that compensates for movement errors resulting from environmental disturbances and from the modeled trajectory generator. This trajectory generator adaptively produces a desired trajectory for a given environmental condition such as a force field. As in Gribble et al. (1998), we model motor adaptation as a change in the desired trajectory. We describe this trajectory modification in the present paper by the weighted sum of basis functions in joint space, in which the weights are updated on a trial-by-trial basis according to a learning rule. Our model also includes changes to somatosensory perception following motor learning as described in Ostry et al. (2010) In particular, it is observed that sensed limb position is altered in a systematic fashion in relation to the direction of the learned force field. By incorporating this adaptive phenomenon in sensory systems, we hope to computationally test the idea that the reason the arm trajectory does not return to that observed prior to learning even after washout trials is because of this adaptation in the somatosensory system.

2 Learning and control scheme

2.1 Purpose and basic ideas

The purpose of this paper is to propose a new model of motor control and learning that explains both human motor learning and associated perceptual change. Humans adopt various strategies for motor control and learning: impedance or stiffness is adjusted for movements early in learning or for movements in unlearnable environments. In other cases, motor commands are adjusted in a highly specific fashion so as to produce desired movements and at the same time anticipate and correct for predictable motion-related forces (such as interaction torques). In the present paper, we consider the situation in which central motor commands are adjusted to achieve a desired movement in the presence of movement-related loads. For modeling purposes, we assume that factors such as impedance are fixed to simplify the control problem without losing its basic characteristics. Figure 1 shows a conceptual block diagram for motor control and learning.

The basic postulates for the proposed model of motor learning are as follows:

P1 A reference trajectory specifying hand position in the workspace is created based upon the task requirements.

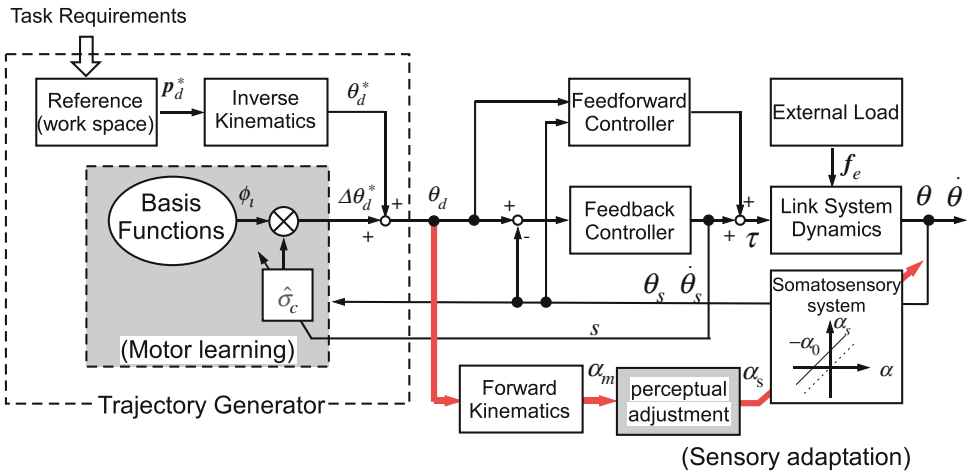

Fig. 1 Control and adaptation scheme for human movement including sensory adaptation

The purpose of the control scheme is to achieve this reference trajectory regardless of the presence of load.

P2 Feedback control of movement occurs in joint space. The assumption is that the reference trajectory in P1 is transformed to joint space to define desired joint-angular trajectories. Desired joint-space trajectories are adjusted to achieve reference trajectories in force-field conditions. These assumptions are consistent with the finding that in the case of dynamics learning, learning occurs in intrinsic coordinates (Malfait et al. 2002; Shadmehr and Mussa-Ivaldi 1994).

P3 A feedforward controller is used to compensate for limb dynamics so as to achieve the desired trajectories. Output torques from both the feedforward and feedback controllers are applied to each joint.

P4 Sensed joint angles and velocities are used to reduce joint angle error in the feedback controller and to compensate the nonlinear effects of arm dynamics in the feedforward controller.

P5 The external loads such as those experienced in force-field learning result in changes in joint space, i.e., the difference between desired and actual joint angles.

P6 Based on errors, the feedback controller works to bring each joint to the desired position. At the same time, desired trajectories are gradually adjusted to decrease errors associated with external loads. As desired trajectories change, error is reduced and the system shifts from feedback to feedforward control (Bhushan and Shadmehr 1999; Slotine and Li 1987).

Note that these postulates are similar in many respects to those of Shadmehr and Mussa-Ivaldi (1994). Our model differs in its goal of trying to capture the dynamics of the learning process. It also differs from the approach proposed by Todorov and Jordan (2002) in which trajectory planning and execution occur simultaneously, whereas in the present paper, the reference trajectory is updated only in a trial-by-trial fashion. As this issue is not central to the present formulation, we make the simplifying assumption that the reference trajectory is a calculated one trial at a time.

Figure 1 also depicts with a bold red line the flow of perceptual change due to motor learning. The following are the postulated characteristics of perceptual change:

P7 The desired trajectory affects sensed limb position and serves to alter perceptual classification.

P8 This perceptual adaptation also affects the perception of joint angle through inverse kinematics.

In summary, external loads such as those experienced in force-field learning result in changes to the desired trajectory, which in return change the perception of limb position. This implies that sensory adaptation depends on the modification of the desired trajectory, in other words, on motor learning (Ostry et al. 2010).

2.2 Assumptions

We have made the following assumptions to simplify the computational description of learning and control in reaching movement.

A1 Arm movement in horizontal plane can be modeled with 2-link dynamics.

A2 All dynamical parameters are known in advance.

A3 Joint angles and velocities are obtained on line.

A4 There are no feedback delays.

A5 Feedback gains and learning rates are constant.

A6 Reference trajectories in the workspace can be achieved by adjusting joint-angular trajectories.

A7 The reference trajectory of the hand is such that the associated desired joint trajectories are bounded and have bounded first and second derivatives.

In the following subsection, motor learning is first analyzed from the stability point of view, without perceptual change (the red line in Fig. 1). In this case, the block "somatosensory system" is treated as an identity transformation. Next, the total control scheme is presented, including perceptual adaptation.

2.3 Mathematical model of motor learning

Human arm motion can be represented as a 2-link system in the horizontal plane as shown in Fig. 2 (A1). The dynamics of the arm is described as follows:

$$M(\boldsymbol{\theta})\ddot{\boldsymbol{\theta}} + C(\boldsymbol{\theta}, \dot{\boldsymbol{\theta}})\dot{\boldsymbol{\theta}} = J^T(\boldsymbol{\theta})\boldsymbol{f}_e + \boldsymbol{\tau} \tag{1}$$

Here, $\boldsymbol{\theta} = \begin{bmatrix} \theta_0 & \theta_1 \end{bmatrix}^T$ is a joint angle vector and $\boldsymbol{\tau} = \begin{bmatrix} \tau_0 & \tau_1 \end{bmatrix}^T$ denotes a torque vector at the corresponding joints, $M(\boldsymbol{\theta})$ is

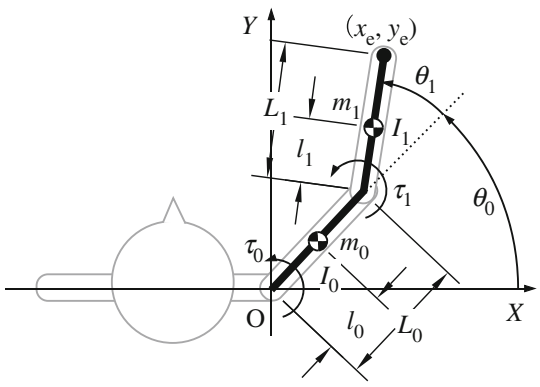

Fig. 2 Planar two-joint model of shoulder and elbow movement. The origin of the workspace is at the right shoulder

the inertia matrix, $C(\boldsymbol{\theta},\dot{\boldsymbol{\theta}})\dot{\boldsymbol{\theta}}$ gives Coriolis and centrifugal forces. Descriptions of the matrix M and C are provided in "Appendix" 1. $\boldsymbol{f}_e$ is the external force applied to the hand. In the present case, the effect of the velocity-dependent force field is modeled as follows, using a viscosity matrix D_p

$$\boldsymbol{f}_e = D_p \begin{bmatrix} \dot{x}_e \\ \dot{y}_e \end{bmatrix} \tag{2}$$

$J(\boldsymbol{\theta})$ is the Jacobian matrix that maps joint velocity to the hand velocity $\begin{bmatrix} \dot{x}_e & \dot{y}_e \end{bmatrix}^T$ and ^{T} denotes the transpose of matrix. See "Appendix" 1 for the Jacobian transformation matrix.

Control input, $\boldsymbol{\tau}$, is defined using the adaptive control scheme proposed by Slotine and Li (1987).

$$\boldsymbol{\tau} = Y_L(\boldsymbol{\theta},\dot{\boldsymbol{\theta}},\dot{\boldsymbol{\theta}}_r,\ddot{\boldsymbol{\theta}}_r)\hat{\boldsymbol{\sigma}}_L - K_d\boldsymbol{s}_o \tag{3}$$

where

$$\dot{\boldsymbol{\theta}}_r = \dot{\boldsymbol{\theta}}_d + K_a(\boldsymbol{\theta}_d - \boldsymbol{\theta}) \tag{4}$$

$$\ddot{\boldsymbol{\theta}}_r = \ddot{\boldsymbol{\theta}}_d + K_a(\dot{\boldsymbol{\theta}}_d - \dot{\boldsymbol{\theta}}) \tag{5}$$

$$\boldsymbol{s}_o = \dot{\boldsymbol{\theta}} - \dot{\boldsymbol{\theta}}_r \tag{6}$$

$\boldsymbol{\theta}_d$ is the desired joint angle vector, K_d and K_a are diagonal positive matrices for feedback gains. Note that this formulation avoids the need to directly measure angular acceleration, $\ddot{\boldsymbol{\theta}}$. The matrix $Y_L(\boldsymbol{\theta},\dot{\boldsymbol{\theta}},\dot{\boldsymbol{\theta}}_r,\ddot{\boldsymbol{\theta}}_r)$ and the vector $\boldsymbol{\sigma}_L$ together satisfy the equation

$$M(\boldsymbol{\theta})\ddot{\boldsymbol{\theta}} + C(\boldsymbol{\theta},\dot{\boldsymbol{\theta}})\dot{\boldsymbol{\theta}} = Y_L(\boldsymbol{\theta},\dot{\boldsymbol{\theta}},\dot{\boldsymbol{\theta}},\ddot{\boldsymbol{\theta}})\boldsymbol{\sigma}_L \tag{7}$$

"Appendix" 1 provides a detailed description of each element of the equation. With the assumption that $\hat{\boldsymbol{\sigma}}_L$ is an estimate of the unknown dynamic parameter vector $\boldsymbol{\sigma}_L$, estimates $\hat{\boldsymbol{\sigma}}_L$ are updated by the following adaptation rule.

$$\dot{\hat{\boldsymbol{\sigma}}}_L = -\Gamma_L Y_L(\boldsymbol{\theta},\dot{\boldsymbol{\theta}},\dot{\boldsymbol{\theta}}_r,\ddot{\boldsymbol{\theta}}_r)^T\boldsymbol{s}_o \tag{8}$$

where Γ_L is a diagonal positive matrix determining the learning rate.

Here, we assume that all of the dynamical parameters are known (A2), and hence, the adaption rule in Eq. (8) is not required. Instead, external velocity-dependent forces have to be considered. Therefore, we modify the scheme for adaptive control as follows:

First, instead of estimating dynamical parameters, we utilize the known true parameter values, $\boldsymbol{\sigma}_L$, in the control law (3).

Next, we introduce the adjustment of the desired trajectories in joint space. We assume that the goal of the control scheme is to achieve straight hand trajectories in workspace (P1), $\boldsymbol{p}_d^*$. Inverse kinematics are used to transform $\boldsymbol{p}_d^*$ to $\boldsymbol{\theta}_d^*$, the desired trajectories in joint space (P2). If $\boldsymbol{f}_e = \boldsymbol{0}$, $\boldsymbol{\theta}_d^*$ achieves $\boldsymbol{p}_d^*$ in hand space. However, when nonzero $\boldsymbol{f}_e$ occurs in the motor learning task, hand trajectories are perturbed and the original controller is prevented from obtaining $\boldsymbol{p}_d^*$ (P5). In this case, the desired trajectories in joint space $\boldsymbol{\theta}_d^*$ must be adjusted to achieve $\boldsymbol{p}_d^*$ (P6). Here, we assume that incremental adjustments to the desired joint angle $\Delta\boldsymbol{\theta}_d^*$ are employed.

$$\boldsymbol{\theta}_d = \boldsymbol{\theta}_d^* + \Delta\boldsymbol{\theta}_d^* \tag{9}$$

Using this equation, we can rewrite (3) by collecting $\Delta\boldsymbol{\theta}_d^*$ terms as follows:

$$\boldsymbol{\tau} = Y_L(\boldsymbol{\theta},\dot{\boldsymbol{\theta}},\dot{\boldsymbol{\theta}}_r^*,\ddot{\boldsymbol{\theta}}_r^*)\boldsymbol{\sigma}_L + \boldsymbol{\tau}_\Delta(\Delta\boldsymbol{\theta}_d^*,\Delta\dot{\boldsymbol{\theta}}_d^*,\Delta\ddot{\boldsymbol{\theta}}_d^*) - K_d\boldsymbol{s} \tag{10}$$

Here,

$$\dot{\boldsymbol{\theta}}_r^* = \dot{\boldsymbol{\theta}}_d^* + K_a(\boldsymbol{\theta}_d^* - \boldsymbol{\theta}) \tag{11}$$

$$\boldsymbol{s} = \dot{\boldsymbol{\theta}} - \dot{\boldsymbol{\theta}}_r^*. \tag{12}$$

The derivation of (10) is given in "Appendix" 2.

The second term on the right-hand side of Eq. (10) acts to compensate for the effects of the force field. In order to describe it, suppose that $\Delta\boldsymbol{\theta}_d^*$ is expanded to the weighted sum of basis functions $\phi_i(t)$ (Ito et al. 2003; Chien and Huang 2004; Ito and Kawasaki 2005)

$$\Delta\boldsymbol{\theta}_d^* = \begin{bmatrix} \Delta\theta_{d0}^* \\ \Delta\theta_{d1}^* \end{bmatrix} = \begin{bmatrix} \sum_{i=1}^n c_{0i}\phi_i(t) \\ \sum_{i=1}^n c_{1i}\phi_i(t) \end{bmatrix} = Y_\phi(t)\boldsymbol{\sigma}_c \tag{13}$$

where

$$Y_\phi(t) = \begin{bmatrix} \phi_1(t) & \cdots & \phi_n(t) & 0 & \cdots & 0 \\ 0 & \cdots & 0 & \phi_1(t) & \cdots & \phi_n(t) \end{bmatrix} \tag{14}$$

$$\boldsymbol{\sigma}_c = \begin{bmatrix} c_{01} & \cdots & c_{0n} & c_{11} & \cdots & c_{0n} \end{bmatrix}^T \tag{15}$$

Substituting $\boldsymbol{\tau}_\Delta$ in Eq. (10) with Eq. (13), we obtain

$$\boldsymbol{\tau} = Y_L(\boldsymbol{\theta},\dot{\boldsymbol{\theta}},\dot{\boldsymbol{\theta}}_r^*,\ddot{\boldsymbol{\theta}}_r^*)\boldsymbol{\sigma}_L + Y_\psi(t)\boldsymbol{\sigma}_c - K_d\boldsymbol{s} \tag{16}$$

where

$$\begin{aligned} Y_\psi(t) &= M(\boldsymbol{\theta})\ddot{Y}_\phi(t) + (M(\boldsymbol{\theta})K_a + C(\boldsymbol{\theta},\dot{\boldsymbol{\theta}}) + K_d)\dot{Y}_\phi(t) \\ &\quad + (C(\boldsymbol{\theta},\dot{\boldsymbol{\theta}}) + K_d)K_aY_\phi(t) \\ &= \begin{bmatrix} \psi_{0,1}(t) & \cdots & \psi_{0,2n}(t) \\ \psi_{1,1}(t) & \cdots & \psi_{1,2n}(t) \end{bmatrix} \end{aligned} \tag{17}$$

See "Appendix" 2 for details.

Here, we assume that the effects of the force field are completely compensated for or offset by the modified desired trajectories $\Delta\boldsymbol{\theta}_d^*$ (A6). Mathematically, this means that $-J^T(\boldsymbol{\theta})\boldsymbol{f}_e$ can be spanned by the functions $\psi_{i,j}(t)$, that is,

$$-J^T(\boldsymbol{\theta})\boldsymbol{f}_e = Y_\psi(t)\boldsymbol{\sigma}_c \tag{18}$$

$\boldsymbol{\sigma}_c$ is not known beforehand. But, using its estimates $\hat{\boldsymbol{\sigma}}_c$, we can define a new control law

$$\boldsymbol{\tau} = Y_L(\boldsymbol{\theta},\dot{\boldsymbol{\theta}},\dot{\boldsymbol{\theta}}_r^*,\ddot{\boldsymbol{\theta}}_r^*)\boldsymbol{\sigma}_L + Y_\psi(t)\hat{\boldsymbol{\sigma}}_c - K_d\boldsymbol{s} \tag{19}$$

and an adaptation rule of the form of Eq. (8) that dynamically estimates values for the vector $\hat{\boldsymbol{\sigma}}_c$:

$$\dot{\hat{\boldsymbol{\sigma}}}_c = -\Gamma Y_\psi^T \boldsymbol{s} \tag{20}$$

where positive definite Γ represents the learning rate. Theorem 1 proves that the hand trajectory converges to its reference $\boldsymbol{p}_d^*$.

Theorem 1 *For the dynamical system described in Eq. (1) with an assumed control law defined by Eq. (19) and an adaptation rule given in Eq. (20), if Eq. (18) holds for the bounded functional system $\psi_{i,j}(t)$, each joint angle converges to its desired trajectory $\boldsymbol{\theta}_d^*$, that is, the actual hand trajectory converges to reference trajectory, $\boldsymbol{p}_d^*$.*

Proof From the definition of Y_L, we get

$$M(\boldsymbol{\theta})\ddot{\boldsymbol{\theta}}_r^* + C(\boldsymbol{\theta},\dot{\boldsymbol{\theta}})\dot{\boldsymbol{\theta}}_r^* = Y_L(\boldsymbol{\theta},\dot{\boldsymbol{\theta}},\dot{\boldsymbol{\theta}}_r^*,\ddot{\boldsymbol{\theta}}_r^*)\boldsymbol{\sigma}_L \tag{21}$$

Subtracting this from (1) gives

$$M(\boldsymbol{\theta})\dot{\boldsymbol{s}} + C(\boldsymbol{\theta},\dot{\boldsymbol{\theta}})\boldsymbol{s} = J^T(\boldsymbol{\theta})\boldsymbol{f}_e + \boldsymbol{\tau} - Y_L(\boldsymbol{\theta},\dot{\boldsymbol{\theta}},\dot{\boldsymbol{\theta}}_r^*,\ddot{\boldsymbol{\theta}}_r^*)\boldsymbol{\sigma}_L \tag{22}$$

Using Eqs. (18) and (19), we can rewrite this as follows:

$$M(\boldsymbol{\theta})\dot{\boldsymbol{s}} + C(\boldsymbol{\theta},\dot{\boldsymbol{\theta}})\boldsymbol{s} = Y_\psi(t)\bar{\boldsymbol{\sigma}}_c - K_d\boldsymbol{s} \tag{23}$$

where

$$\bar{\boldsymbol{\sigma}}_c = \hat{\boldsymbol{\sigma}}_c - \boldsymbol{\sigma}_c \tag{24}$$

Now, consider the following positive definite function

$$V = \frac{1}{2}\boldsymbol{s}^T M(\boldsymbol{\theta})\boldsymbol{s} + \frac{1}{2}\bar{\boldsymbol{\sigma}}_c^T \Gamma^{-1}\bar{\boldsymbol{\sigma}}_c \tag{25}$$

The derivative of V is

$$\dot{V} = \boldsymbol{s}^T M(\boldsymbol{\theta})\dot{\boldsymbol{s}} + \frac{1}{2}\boldsymbol{s}^T \dot{M}(\boldsymbol{\theta})\boldsymbol{s} + \dot{\hat{\boldsymbol{\sigma}}}_c^T \Gamma^{-1}\bar{\boldsymbol{\sigma}}_c \tag{26}$$

Substituting $M(\boldsymbol{\theta})\dot{\boldsymbol{s}}$ from Eq. (23) in Eq. (26) and since $\dot{M} - 2C$ is the skew symmetry matrix that satisfies $\boldsymbol{s}^T(\dot{M} - 2C)\boldsymbol{s} = 0$ for any vector $\boldsymbol{s}$, we get

$$\dot{V} = -\boldsymbol{s}^T K_d \boldsymbol{s} + [\boldsymbol{s}^T Y_\psi(t) + \dot{\hat{\boldsymbol{\sigma}}}_c^T \Gamma^{-1}]\bar{\boldsymbol{\sigma}}_c. \tag{27}$$

With the adaptation rule of Eq. (20), the second term of the right-hand side of Eq. (27) is eliminated and $\dot{V}$ becomes positive semi-definite as follows:

$$\dot{V} = -\boldsymbol{s}^T K_d \boldsymbol{s} \tag{28}$$

Furthermore, $\ddot{V}$ becomes

$$\ddot{V} = -2\boldsymbol{s}^T K_d \dot{\boldsymbol{s}} \tag{29}$$

We can ensure the boundedness of $\ddot{V}$ as described in "Appendix" 3. Therefore, from the Lyapunov-like lemma, $\dot{V}$ converges to zero, implying $\boldsymbol{s} \to \boldsymbol{0}$ and thus $\boldsymbol{\theta} \to \boldsymbol{\theta}_d^*$. Because $\boldsymbol{\theta}_d^*$ is calculated from the hand reference trajectory $\boldsymbol{p}_d^*$, if the controller realizes $\boldsymbol{\theta}_d^*$ the hand trajectory will follow $\boldsymbol{p}_d^*$. □

Note 1 The above theorem does not always ensure $\bar{\boldsymbol{\sigma}}_c \to \boldsymbol{0}$, that is, that estimates of $\boldsymbol{\sigma}_c$ converge to their true values $\boldsymbol{\sigma}_c$. If another solution exists such that $\boldsymbol{\theta} \to \boldsymbol{\theta}_d^*$, $\Delta\boldsymbol{\theta}_d^*$ may converge to this solution instead of the true one. It is known that, in order for the estimates to approach their true values, persistent excitation is required (Slotine and Li 1991), implying that a broad sampling of reference trajectories is necessary.

Note 2 The control law (19) can be rewritten as follows:

$$\begin{aligned}\boldsymbol{\tau} = {} & Y_L(\boldsymbol{\theta},\dot{\boldsymbol{\theta}},\dot{\boldsymbol{\theta}}_r^* + \Delta\dot{\boldsymbol{\theta}}_r^*,\ddot{\boldsymbol{\theta}}_r^* + \Delta\ddot{\boldsymbol{\theta}}_r^*)\boldsymbol{\sigma}_L \\ & + [K_d((\dot{\boldsymbol{\theta}}_d^* + \Delta\dot{\boldsymbol{\theta}}_d^*) - \dot{\boldsymbol{\theta}}) + K_p((\boldsymbol{\theta}_d^* + \Delta\boldsymbol{\theta}_d^*) - \boldsymbol{\theta})]\end{aligned} \tag{30}$$

where $K_p = K_d K_a$. The first term corresponds to the output of the feedforward controller (P3), and the second term describes the feedback (PD) controller (P2). The only feedback inputs to the controllers are joint angles and velocities (P4).

2.4 Modeling of perceptual change

We wish to focus on the characteristics of the washout phase and, in particular, on a characteristic of learning that is also observed empirically, the failure to return to straight movement at the end of washout trials. We consider two possibilities. One, of course, is that the effect is due to the small number of trials in the washout phase and hence the inability to return to a straight movement path given the large time constant for adaptation and de-adaptation. A second possibility is that the persistent error at the end of washout reflects recent evidence that learning results in changes in somatosensory function.

Before tackling this question, we consider how we might introduce somatosensory perceptual change into our model. Empirically, changes in somatosensory function in association with motor learning are reflected in changes in the perception of limb position (Ostry et al. 2010). One possibility is that the perceptual change may be related to changes in the desired trajectory over the course of learning. In our model, desired trajectories are curved in a direction opposite to the applied force, for example, to the right for counterclockwise loads. Thus, it is possible that the direction the hand is intended to move affects the perception of limb position: The movement target in this experiment was chosen so as to lie in the sagittal plane, straight out along the midline of the body, and thus coincides with the direction of the geometrical boundary between the right and left side of the workspace. Learning results in a shift in the perceptual boundary in the direction of the intended movement (or virtual target), which is opposite to the direction of the force applied by the robot.

An alternative possibility that the distributional characteristics of experienced movements can account for the proposed perceptual change will be difficult to reconcile with

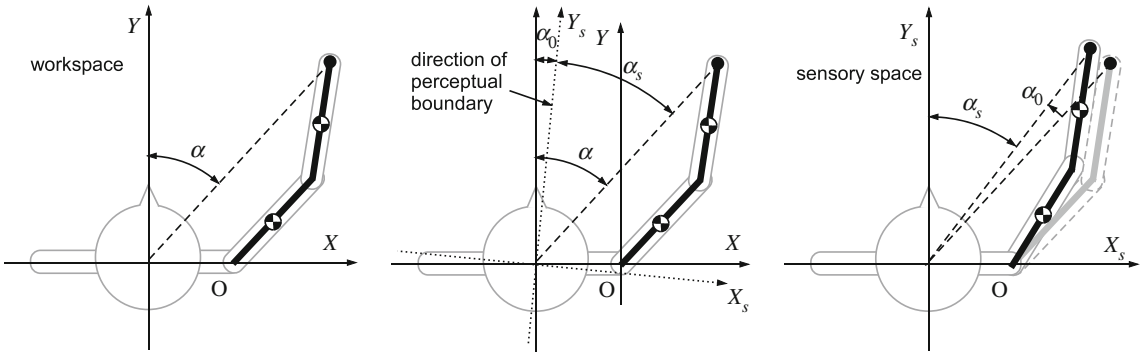

Fig. 3 Change in perceptual boundary affects sensed joint angles

the empirically observed pattern of perceptual shift. Whereas the perceptual shift coincides with the "desired" movement direction, the area of the workspace that is experienced kinematically during training is in the opposite direction, that is, on the other side of the body midline. Accordingly, it seems reasonable to assume that the system uses the desired or reference trajectory as a basis for perceptual change (P7). Based on this idea, we propose that the process of perceptual change occurs in the following manner. Assume that the orientation or direction of the desired hand trajectory relative to a straight line from movement start to end is α_m. The associated perceptual boundary orientation is $\alpha_0(i)$, which is updated discretely after each trial as follows:

$$\alpha_0(i+1) = \alpha_0(i) + k_s(\alpha_m(i) - \alpha_0(i)) \tag{31}$$

namely on the basis of the difference in orientation between the desired movement and the current perceptual boundary. k_s is a constant that determines the speed of the perceptual change and i denotes the trial number. During each trial, α_0 remains constant.

For the calculation of $\alpha_m(i)$, the velocity-weighted average of movement direction ξ is computed

$$\alpha_m(i) = \frac{\int_{t_s}^{t_f} v_e^d \xi \, \mathrm{d}t}{\int_{t_s}^{t_f} v_e^d \mathrm{d}t} \tag{32}$$

where

$$\xi = \mathrm{atan2}(\dot{x}_e^d, \dot{y}_e^d) \tag{33}$$

$$v_e^d = \sqrt{(\dot{x}_e^d)^2 + (\dot{y}_e^d)^2} \tag{34}$$

and $\dot{x}_e^d$ and $\dot{y}_e^d$ represent desired hand velocity. This formulation weights most highly the directions in the trajectory in which instantaneous desired velocity is high. As the range of integration, we selected the period of intended movement, that is, the period over which the reference trajectory has nonzero velocity, from t_s to t_f.

To incorporate this perceptual boundary shift into a model of limb control, we consider the change in the sensed limb configuration in intrinsic or joint coordinates based on P8. To describe this change, α and α_s are introduced, which, respectively, denote the hand orientation in the real work space and in sensory space, as shown in Fig. 3. On the assumption that the distance to the hand remains constant, a change in the orientation of the perceptual boundary, α_0, actually corresponds to a change in α_s

$$\alpha_s = \alpha - \alpha_0 \tag{35}$$

In other words, the center of the sensory coordinate system is rotated by $+\alpha_0$ with respect to the body midline and accordingly hand position is sensed as if it had rotated by $-\alpha_0$. Each of the sensed joint angles $\boldsymbol{\theta}_s$ associated with these perceptual changes is obtained by solving the inverse kinematics. The control law (19) and the adaptation rule (20) can be rewritten using $\boldsymbol{\theta}_s$ instead of $\boldsymbol{\theta}$.

3 Computational studies

3.1 Purpose and conditions

The main purpose of the simulations is to determine whether the computational model proposed in the previous section can reproduce characteristics of human motor learning, both qualitatively or quantitatively, including the fact that hand trajectories do not return to baseline levels following washout trials.

A typical human motor learning experiment involving arm movement has three phases: a null field phase in which the subject makes reaching movements in the absence of load while holding the handle of a robotic device (A), a force-field training phase in which the robot applies forces in a lateral direction in proportion to the tangential velocity of the hand (B), and a final null field phase in which the effects of learning are "washed out" (C). The force field is defined by the following equation,

$$\boldsymbol{f}_e = D \begin{bmatrix} 0 & 1 \\ -1 & 0 \end{bmatrix} \begin{bmatrix} \dot{x}_e \\ \dot{y}_e \end{bmatrix} \tag{36}$$

where D is the magnitude of the force field in N s/m. As in experiments with human subjects, reaching movements are simulated in a repeated manner: on each trial, the hand moves from start position $\boldsymbol{p}_s$ at t_s[s] to target position $\boldsymbol{p}_f$ at t_f[s]. The total trial duration is T_{trial}. In each successive trial, all initial values are the same, except the learning parameter $\hat{\boldsymbol{\sigma}}_c$, which is updated based on the previous trial.

As a first step, the converge of the control algorithm is confirmed. Next, the motor learning with perceptual adaptation is simulated.

3.2 Parameters

We simulated a series of 350 reaching movements in a single straight ahead direction: There were 150 movements in each of the null field and force-field conditions (Phases A and B, respectively) and 50 additional washout trials, again under null field conditions (Phase C). The force-field strength parameter was set to +18 N s/m for the clockwise curl field and −18 N s/m the counterclockwise field. Namely, D in (36) was set to 0 in Phase A and Phase C. D was set to −18 N s/m for the convergence analysis described above in Theorem 1.

The physical parameters of the two-joint arm model (see Fig. 2) were set to the following values, based on Shadmehr and Mussa-Ivaldi (1994) and Tee et al. (2010); $m_0 = 1.93\,\text{kg}$, $m_1 = 1.52\,\text{kg}$, $\ell_0 = 0.165\,\text{m}$, $\ell_1 = 0.190\,\text{m}$, $L_0 = 0.31\,\text{m}$, $L_1 = 0.34\,\text{m}$, $I_0 = 0.0141\,\text{kg m}^2$, $I_1 = 0.0188\,\text{kg m}^2$. The parameters corresponding to feedback gains were set as $K_d = \text{diag}(2.5, 2.5)\,\text{Nm s}$, $K_a = \text{diag}(6, 6)\,\text{s}^{-1}$.

The reference trajectories were modeled as fifth-order polynomials following a minimum jerk trajectory. Movement start and end positions were set at $\boldsymbol{p}_s = (-0.20,\ 0.20\,\text{m})$, $\boldsymbol{p}_f = (-0.20, 0.40\,\text{m})$. The duration of the each trial was set to $T_{\text{trial}} = 5\,\text{s}$. The limb remained at the start position until $t_s = 1.2\,\text{s}$ and produced a movement to the target that ended at $t_f = 2.0\,\text{s}$. The limb remained at the target for the remainder of the trial.

Gaussian basis functions were used to model the pattern of movement error over the course of learning.

$$\phi_j(t) = \exp[-c(t - j \times \Delta t)^2] \tag{37}$$

$$\Delta t = T_{\text{trial}}/(n-1) \tag{38}$$

n is the number of functions; the functions are equally spaced over the simulated movement time. c changes the width of the function. Since $\dot{\phi}(t)$ and $\ddot{\phi}(t)$ are bounded, the boundedness of $Y_\psi(t)$ is ensured.

For the numerical integration, a fourth-order Runge–Kutta algorithm is used with a 0.001 s time step.

3.3 Convergence

Satisfying Eq. (18) depends on the number of the basis functions, n. Here, we have examined the convergence of hand trajectory to its reference from this point of view. Although the iterative application of the control law and learning rule do not always ensure convergence (because Theorem 1 assumes continuity of time), we have obtained stable results from the simulations. Figure 4 shows simulations that assess convergence using three values for the number of basis functions, n. Each panel shows simulated hand paths and velocity profiles over the course of learning (trials 1–200). Panel (a) shows the result with a small number of functions, $n = 3$ and $c = 2$. Panel (b) gives an intermediate case with $n = 26$ and $c = 5$. Panel (c) shows the result with a large number of functions, $n = 251$ and $c = 15$.

All three simulations show some common features. Early in learning movements are curved to the left and have velocity profiles with multiple peaks. When the number of basis functions is low, the simulated movements remain deviated from the desired trajectory, indicating that the controller cannot converge to the reference. In (b), acceptable results are obtained: with training, the hand path becomes increasingly straight and the velocity profile becomes bell-shaped, although ripples are observed at the end of movement when velocity is low. In panel (c), almost perfect learning is accomplished; velocity profiles quickly become bell-shaped. The results indicate that for large n, the proposed control algorithm successfully achieves the reference trajectory.

3.4 Reproducing human behavior

Our model can fully learn the force field if we choose a large n. This can be seen in Fig. 4c for an n of 251. However, empirical studies show that subjects do not fully compensate for the force field in only 150 trials of training. In Ostry et al. (2010), it can be seen that the perpendicular displacement (PD) of the hand relative to a straight line from start to end positions remains deviated to the right in the clockwise force field and to the left in the counterclockwise force field after 150 training trials (see Fig. 5a). The difference of PD values between left and rightward force fields is about 20 mm at the end of the training Phase B. The difference is present even after the washout Phase C. It reaches about 6 mm after 50 washout trials. To reproduce the Phase B empirical results, we set $n = 13$ and $c = 6$. We used a learning rate of $\Gamma = \text{diag}[3.5 \times 10^{-6}, \ldots, 3.5 \times 10^{-6}]$ and a perceptual change rate of $k_s = 2.0 \times 10^{-4}$ to fit the Phase C results. These parameters were used throughout the simulations described in this section.

Figure 6 shows simulated hand paths under null, force-field, and washout conditions, for movements in counterclockwise (upper panel) and clockwise force fields

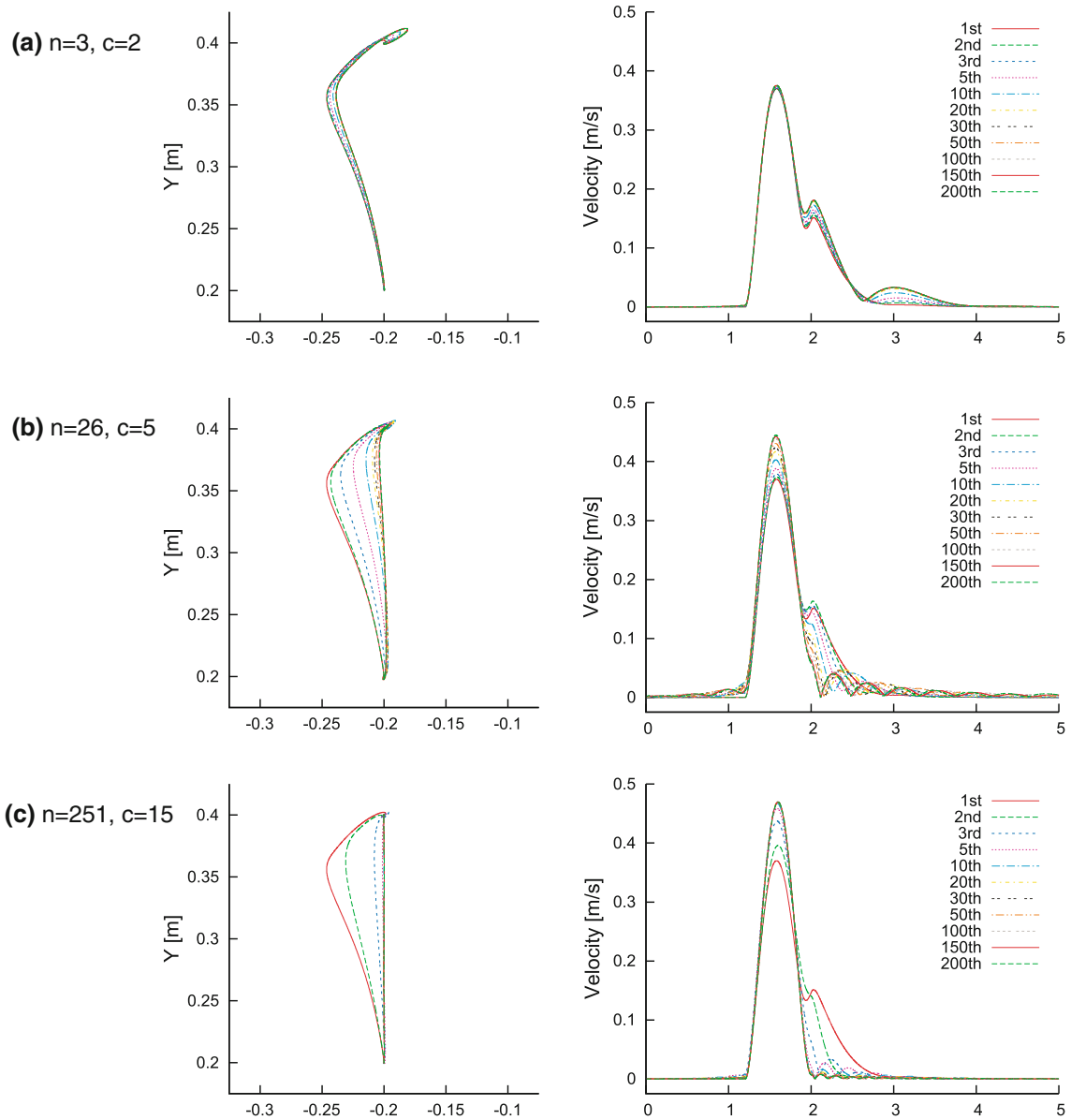

Fig. 4 Tests for the convergence of simulated hand position and velocity in force-field learning. *n* represents the number of Gaussian basis functions used to represent joint deviation during learning. *c* gives the width of the associated basis functions

(lower panel). Under null field conditions, the reference trajectory, which is given as the straight line, is achieved since all the dynamic parameters are known. During force-field trials (Phase B), trajectories are curved, but as motor learning progresses, the observed hand trajectories approach straight line paths. When the force field is removed (Phase C), the hand path is curved in a direction opposite to the force field. Over the course of washout trials, hand paths again approach a straight movement.

As a measure of learning, we computed on a trial-by-trial basis the maximal lateral deviation of the hand from a straight line path. Figure 5b shows values for this measure over the course of learning. Movements in a counterclockwise force field are shown with circles; movements in the clockwise are given with squares. During null field movements in Phase A, paths are entirely straight. When the force field is introduced at the start of the Phase B, an initial lateral deviation of more than 0.040 m is observed for both force-field directions. These deviations decrease to +0.0078 m (CW) and −0.0066 m (CCW) by the end of force-field learning. Aftereffect movements in Phase C are curved in a direction opposite to that observed during learning. An initial lateral deviation of about 0.040 m in aftereffect trials is gradually reduced during washout, but does not go back to zero by the end of the Phase C, that is, after 50 washout trials (−0.0021 for CW and 0.0018 m for CCW).

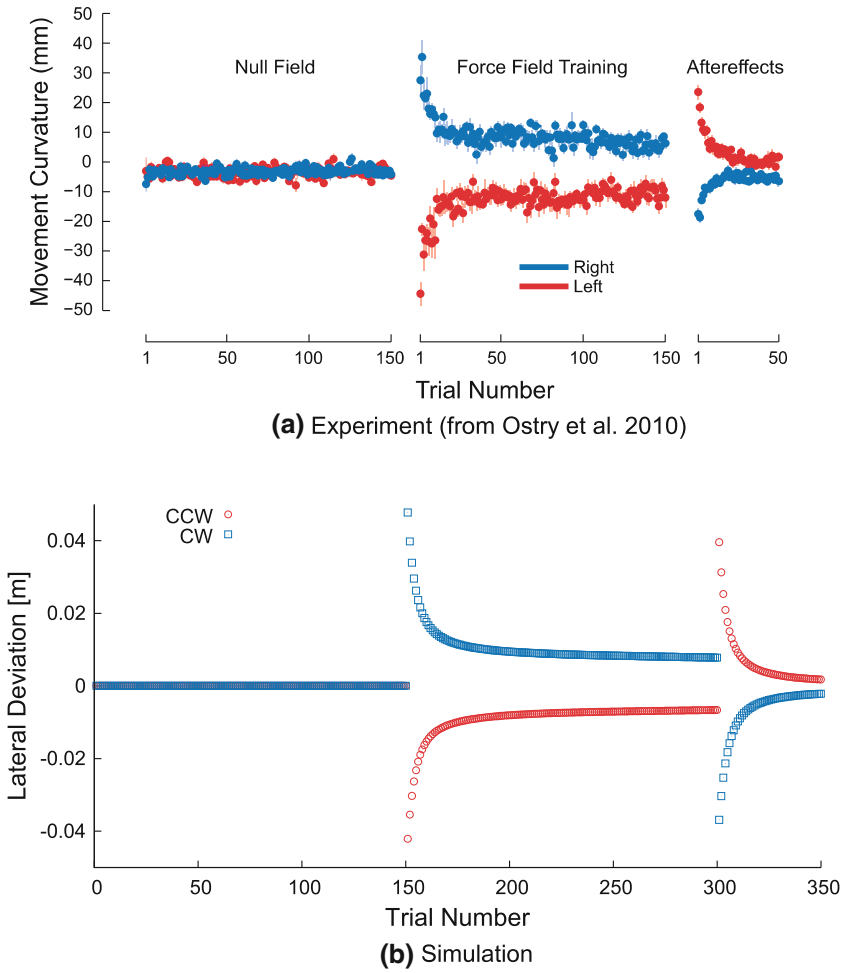

Fig. 5 Maximum lateral deviation over the course of learning

We assessed the similarity of the simulation results to the empirical force-field learning data by fitting, as in Davidson and Wolpert (2004), a discrete form of the exponential function, $c_1 + c_2(1 - c_3)^i$ to the data shown in Fig. 5a, b, where c_1, c_2, and c_3 are fitting parameters, and i is the trial number. We conducted statistical tests for differences in the estimated slope parameter, c_3, in each phase of the experiment and each force-field direction separately. We found no statistically reliable differences in the estimated learning rates between functions fit to the real and simulation data in neither the force-field training nor aftereffect phases of the experiment (Table 1). This suggests that present computational model provides an adequate fit to the empirical results.

Figure 7 shows simulated values of the desired hand trajectory derived using forward kinematics from the desired trajectories of joint angles, that is, $\boldsymbol{\theta}_d^* + \Delta\boldsymbol{\theta}_d^*$, where $\Delta\boldsymbol{\theta}_d^*$ represents changes in desired joint configuration as a result of learning. This desired workspace trajectory reflects the change of the intended movement direction of the hand that causes the perceptual boundary shift. Simulated changes in the perceptual boundary, α_0, are depicted in Fig. 8b, where the rate of perceptual change is set to $k_s = 2.0 \times 10^{-4}$. With these values, the perceptual shift reaches -0.0070 rad for the CW force field and 0.0054 rad for the CCW force field by the end of Phase B. This corresponds to a shift of -1.4 mm (CW) and 1.1 mm (CCW) at the target position, which is 20 cm from the start. The difference between these values is around 2.5 mm, which is similar to the actual shift of the perceptual boundary obtained in experimental studies (Fig. 8a).

3.5 Effect of perceptual change on subsequent movements

In order to assess the effect of perceptual change on arm reaching movements, we simulated 1,300 movements such that the initial null and force-field phases of training stayed the same as before (Fig. 5) and were then followed by 1,000 simulated washout trials (Phase C'). The predicted patterns of motor learning as assessed by the lateral deviation of the hand during learning are shown in Fig. 9. The upper panel (Fig. 9a) shows the simulation with the perceptual change parameter set to $k_s = 2.0 \times 10^{-4}$ (see Eq. (31)). The lower

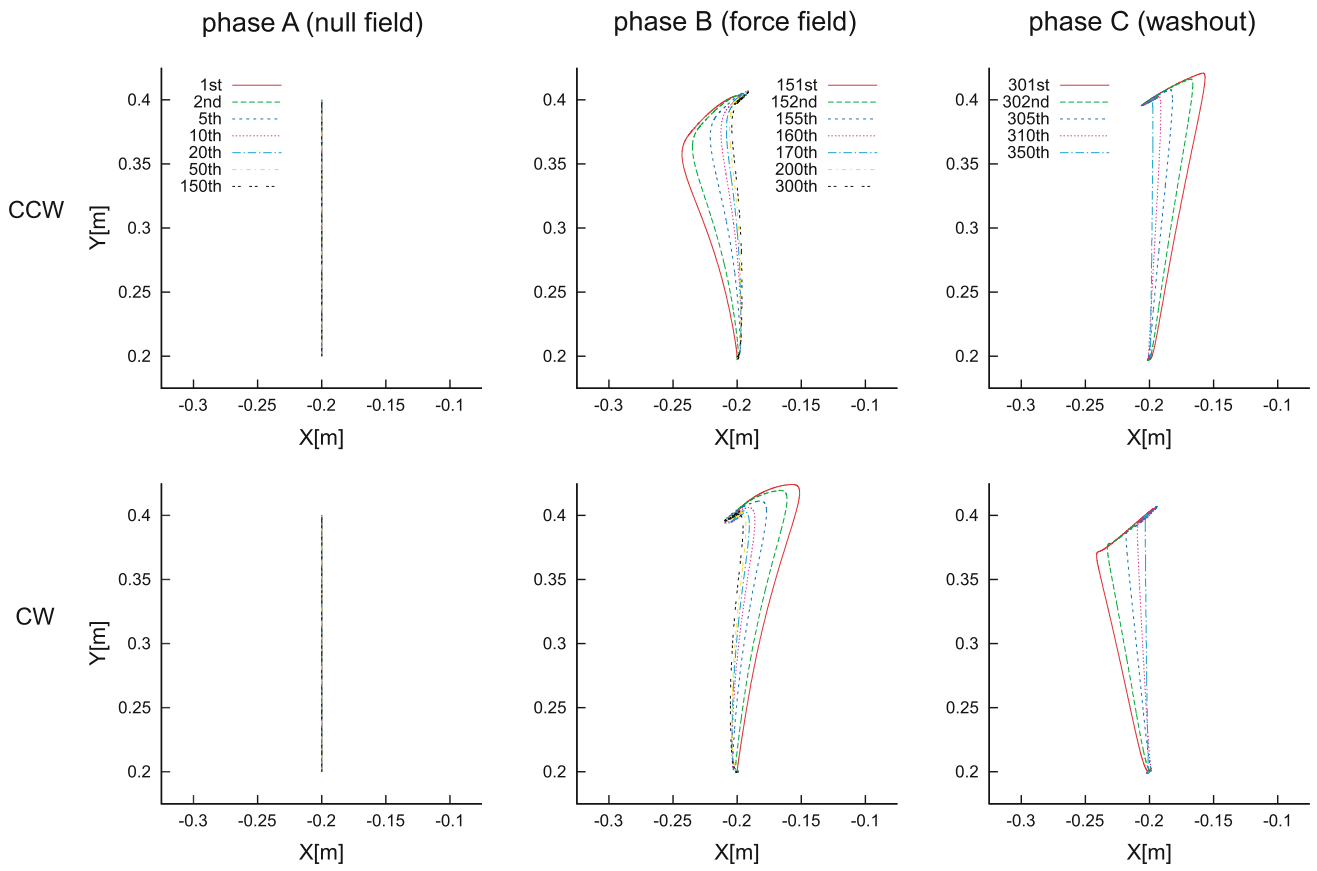

Fig. 6 Simulated hand path during force-field learning. The *top row* shows movements in a counterclockwise force field. The *bottom row* shows a clockwise field. Trial numbers are shown in each panel

Table 1 Estimated rate parameters, c_3, for force-field learning (Phase B) and washout (Phase C) for empirical and simulated results

	Phase B			Phase C		
	Mean	(99 % CI)		Mean	(99 % CI)	
Human (CCW)	0.134	(0.0975	0.1711)	0.140	(0.1092	0.1712)
Simulated (CCW)	0.134	(0.1247	0.1431)	0.174	(0.1619	0.1864)
Human (CW)	0.138	(0.1026	0.1732)	0.213	(0.1561	0.2700)
Simulated (CW)	0.133	(0.1242	0.1418)	0.158	(0.1491	0.1675)

panel (Fig. 9b) presents the case in which the effect of the perceptual boundary shift on motor learning is assumed to be zero ($k_s = 0$). It can be seen that in comparison with the case in which learning results in no change in sensory function ($k_s = 0$), it takes longer time for the hand trajectories to become straight again as a result of the sensory adjustment.

Although not shown here, up to 350 movements, the actual and desired hand path for $k_s = 0$ was almost the same as in Figs. 6 and 7. The effects of including perceptual change in the simulations were rather small, around 1 millimeters, in comparison with the scale of the hand paths shown in these figures.

The predicted perceptual changes are shown in Fig. 10, along with changes in α_m, the desired movement direction. According to (31), the perceptual boundary, α_0, is updated on a trial-by-trial basis depending on the difference between α_m and α_0. When Phase B starts, α_m increases in conjunction with motor learning. When Phase C begins and the force field is removed, α_m returns to zero. At the same time, during Phase B, α_0 gradually evolves toward α_m. However, due to large time constant, α_0 changes slowly. When the Phase C starts and α_m returns to zero, the error that drives the update of α_0 is small in comparison with that in the Phase B, which results in a slow return to baseline for α_0. Accordingly, the large time constant for α_0 dynamics with respect to that of α_m is a reason why the change in α_0 is fast in the Phase B and slow in Phase C. This mechanism explains why the perceptual boundary shifts persist even after washout trials.

These results are consistent with the idea that trajectories do not return to straight not only because of the time constant of motor learning but also because of sensory adjustment, that is, perceptual change in conjunction with motor learning, as well as the rate of de-adaptation both contribute to the incomplete washout that is observed.

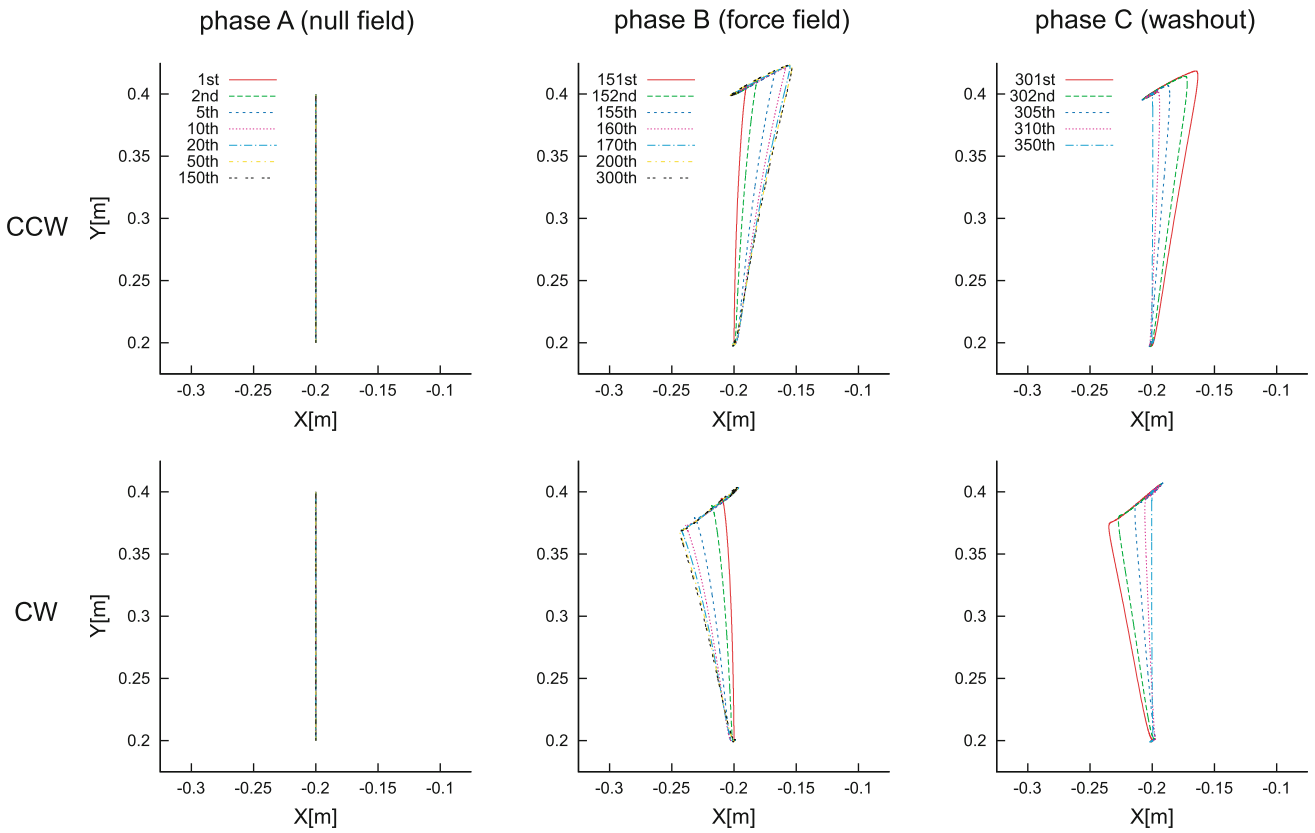

Fig. 7 Desired hand trajectory over the course of learning. *Upper panel* is for counterclockwise loads. *Lower panel* is for clockwise loads

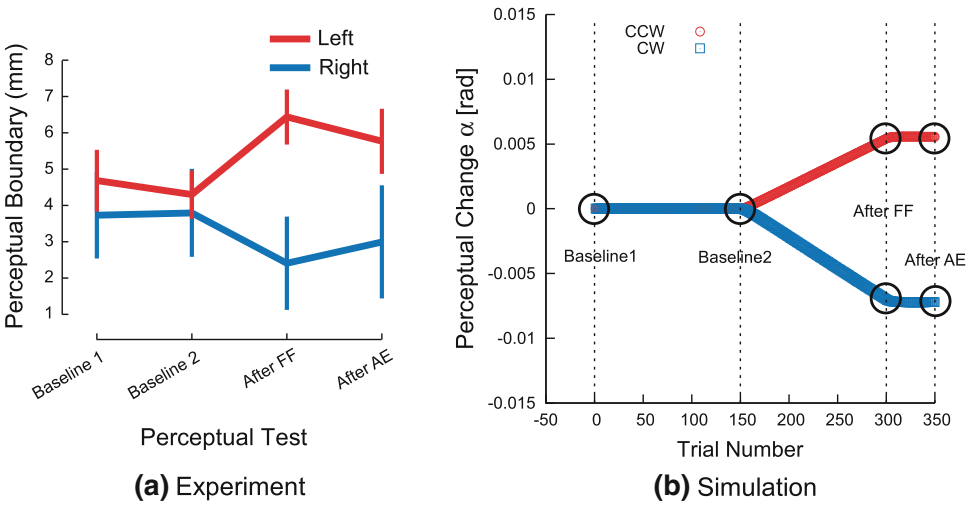

Fig. 8 Perceptual change. *Red* shows perceptual change in association with counterclockwise loads. *Blue* indicates perceptual change for clockwise loads. **a** Human empirical data from Ostry et al. (2010). **b** Simulated perceptual change over the course of learning as represented by the angle α_0

4 Discussion

We have simulated human reaching movement in the presence of external loads. In addition to providing a computational mechanism for adaptation to load, our simulations have focused on two specific characteristics of learning: (i) the curvature of the hand trajectory does not return to a straight line path when the force field is removed, even after many washout trials; (ii) the sensed position of the limb is altered by motor learning. To explain the mechanism behind these characteristics, we have proposed a control and learning scheme in which joint angles are selected as the control variables and motor learning is described in terms of the adjustment of their desired trajectories. The deviation in joint space of desired trajectories from the reference trajectory (translated to joint space using inverse kinematics) is represented as the

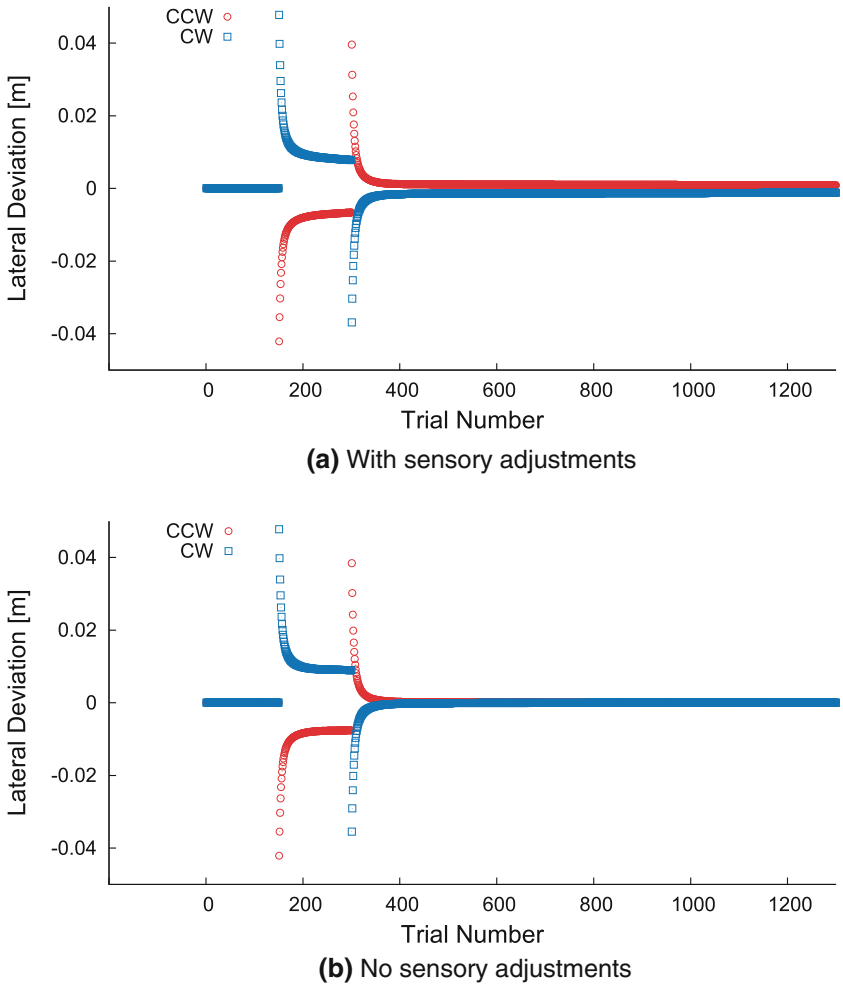

Fig. 9 Predicted hand deviation during learning with (*top panel*) and without (*bottom panel*) sensory change. Each panel shows null trials, force-field learning, and then an extended period of washout in the absence of load

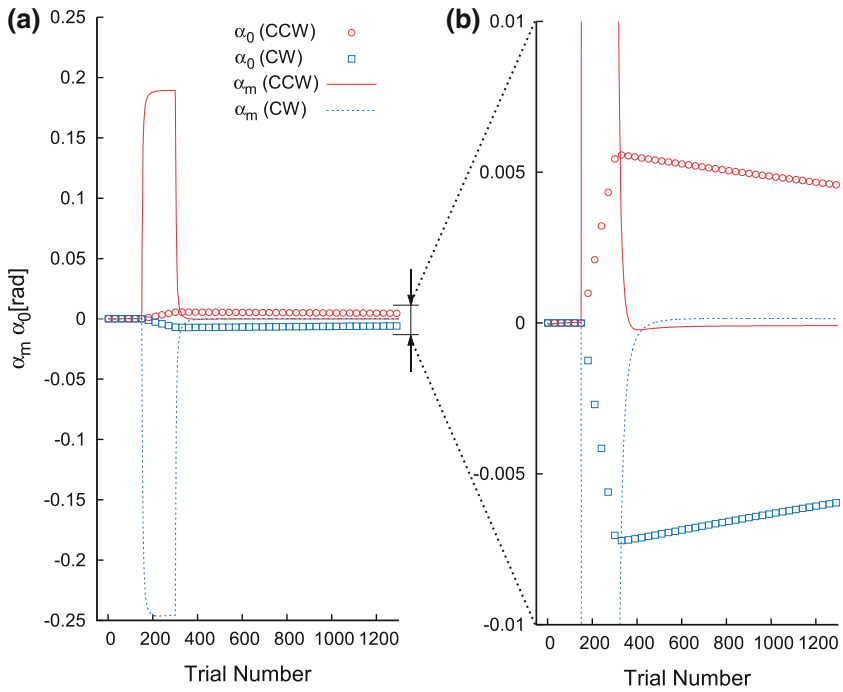

Fig. 10 The change of α_0 in every 30 trials during 1,300 trial simulations. *Red* represents the results for CCW force field *while blue* represents CW force field. The trial-by-trial changes in α_m are overlaid at the same graph. **a** shows a whole evolutions, and **b** is a enlargement of **a** around $\alpha_0 = 0$

weighted sum of Gaussian basis functions whose coefficients are updated to achieve the hand reference trajectory, which is determined on the basis of task requirements. The convergence of the hand trajectory to its reference is guaranteed using a Lyapunov-like lemma and is demonstrated by simulations that estimate the number of the basis functions needed to replicate empirical adaptation.

In order to incorporate changes to somatosensory perception, we considered possible effects of learning on sensory function as a result of changes in desired hand-space trajectories. Empirically, it is seen that the direction of movement coincides with the perceptual boundary and does so both before and after learning, that is, following learning, movements follow altered perceptual boundaries. Consistent with this observation, modeled sensory perception was adjusted after each trial based on changes in the direction of the desired trajectory. Computer simulations demonstrated that sensory adjustments based on this idea have an effect of producing simulated movements that correspond to the shifted perceptual boundary.

The idea that changes to the desired movement trajectory propagate into sensory function is similar in certain respects to the notion of efference copy—the finding that there is sensory change, usually sensory suppression, that is observed in conjunction with voluntary movement (Bernier et al. 2009). The effects that we see and the postulated changes in our model may have ties to efference copy but are different in important respects. First, the modeled perceptual changes (and those observed empirically) are spatial shifts in perceptual function, not perceptual suppression. Second, empirical demonstrations of efference copy-like phenomenon are largely linked to ongoing movement. When the movement ends, perceptual function is restored to former levels. In contrast, the perceptual changes observed in association with motor learning are durable.

We propose a new strategy for motor learning. In our view, the feedforward controller is used to anticipate and correct for limb mechanical behavior. Arm dynamics change slowly and are dependent on factors, such as growth or aging. Persistent use of tools or prostheses can likewise induce changes in feedforward control. Since these factors are outside of the scope of the present study, we assume that feedforward control is unchanged. Adaptation to more transient loads such those involved in force-field adaptation occurs, in our model, through changes to desired arm trajectories.

From the modeling point of view, only one reference trajectory was examined in the present paper. However, the same basic formulation, can be generalized to model movements to other directions and to learning various trajectories at the same time. Humans also show modest generalization of learning to new movement directions. Producing a learning rule that replicates human patterns of generalization would be a valuable future direction. The possibility that adaptation and de-adaptation are characterized by different time constants (Davidson and Wolpert 2004) is a further phenomenon in human motor learning appropriate for further exploration as this would affect predicted characteristics of sensory change during the washout phase. It would also be worthwhile to direct our attention to the possible effects of time delay, redundancy, and the control of arm impedance on the performance of our model.

Acknowledgments This research was supported by the National Institute of Child Health and Human Development (R01-HD075740) and by Le Fonds Quebecois de la Recherche sur la Nature et les Technologies (Quebec).

Conflict of interest The authors declare that they have no conflict of interest.

5 Appendix 1: 2-link system dynamics and kinematics

The 2-link dynamics of the arm in the horizontal plane are described as follows:

$$M(\boldsymbol{\theta})\ddot{\boldsymbol{\theta}} + C(\boldsymbol{\theta}, \dot{\boldsymbol{\theta}})\dot{\boldsymbol{\theta}} = \boldsymbol{\tau} \tag{39}$$

Here, $M(\boldsymbol{\theta})$ and $C(\boldsymbol{\theta}, \dot{\boldsymbol{\theta}})$ are given as follows:

$$M(\boldsymbol{\theta}) = \begin{bmatrix} M_{11} & M_{12} \\ M_{21} & M_{22} \end{bmatrix} \tag{40}$$

$$C(\boldsymbol{\theta}, \dot{\boldsymbol{\theta}}) = \begin{bmatrix} C_{11} & C_{12} \\ C_{21} & C_{22} \end{bmatrix} \tag{41}$$

$$M_{11} = I_0 + I_1 + m_0\ell_0^2 + m_1L_0^2 + m_1\ell_1^2 + 2m_1L_0\ell_1\cos\theta_1 \tag{42}$$

$$M_{12} = M_{21} = I_1 + m_1\ell_1^2 + m_1L_0\ell_1\cos\theta_1 \tag{43}$$

$$M_{22} = I_1 + m_1\ell_1^2 \tag{44}$$

$$C_{11} = -m_1L_0\ell_1\dot{\theta}_1\sin\theta_1 \tag{45}$$

$$C_{12} = -m_1L_0\ell_1(\dot{\theta}_0 + \dot{\theta}_1)\sin\theta_1 \tag{46}$$

$$C_{21} = m_1L_0\ell_1\dot{\theta}_0\sin\theta_1 \tag{47}$$

$$C_{22} = 0 \tag{48}$$

As shown in Fig. 2, θ_i denotes joint angle, L_i is link length, ℓ_i is the distance to center of mass of the link, m_i is mass of the link, I_i is the moment of inertia about the center of mass, τ_i denotes joint torque and i distinguishes the shoulder ($i = 0$) and the elbow ($i = 1$). The operation $\dot{}$ denotes time derivative.

Note here that the left side of Eq. (39) can be described as the product of Y_L and $\boldsymbol{\sigma}_L$ as shown in (7). In the case of 2-link arm dynamics, they are given as

$$Y_L(\boldsymbol{\theta}, \dot{\boldsymbol{\theta}}, \dot{\boldsymbol{\theta}}_r, \ddot{\boldsymbol{\theta}}_r) = \begin{bmatrix} \ddot{\theta}_{r0} & (\ddot{\theta}_{r0} + 2\ddot{\theta}_{r1})\cos\theta_1 + \dot{\theta}_{r1}(2\dot{\theta}_0 + \dot{\theta}_1)\sin\theta_1 & \ddot{\theta}_{r1} \\ 0 & 2\ddot{\theta}_{r0}\cos\theta_1 - \dot{\theta}_{r0}^2\sin\theta_1 & \ddot{\theta}_{r0} + \ddot{\theta}_{r1} \end{bmatrix} \tag{49}$$

$$\boldsymbol{\sigma}_L = \left[\, \sigma_{L1}\ \sigma_{L2}\ \sigma_{L3} \,\right]^T \tag{50}$$

$$\sigma_{L1} = I_0 + I_1 + m_0\ell_0^2 + m_1 L_0^2 + m_1\ell_1^2 \tag{51}$$

$$\sigma_{L2} = m_1 L_0 \ell_1 \tag{52}$$

$$\sigma_{L3} = I_1 + m_1\ell_1^2 \tag{53}$$

Then, the following equation holds using $\hat{\boldsymbol{\sigma}}_L$:

$$Y_L(\boldsymbol{\theta}, \dot{\boldsymbol{\theta}}, \dot{\boldsymbol{\theta}}_r, \ddot{\boldsymbol{\theta}}_r)\hat{\boldsymbol{\sigma}}_L = \hat{M}(\boldsymbol{\theta})\ddot{\boldsymbol{\theta}}_r + \hat{C}(\boldsymbol{\theta}, \dot{\boldsymbol{\theta}})\dot{\boldsymbol{\theta}}_r \tag{54}$$

$\hat{M}(\boldsymbol{\theta})$ and $\hat{C}(\boldsymbol{\theta}, \dot{\boldsymbol{\theta}})$, the estimates of $M(\boldsymbol{\theta})$ and $C(\boldsymbol{\theta}, \dot{\boldsymbol{\theta}})$, respectively.

On the other hand, the relationship between hand position and joint angles is given as follows:

$$x_e = L_0 \cos\theta_0 + L_1 \cos(\theta_0 + \theta_1) \tag{55}$$

$$y_e = L_0 \sin\theta_0 + L_1 \sin(\theta_0 + \theta_1) \tag{56}$$

Hand velocity are related to joint velocities by the Jacobian matrix $J(\boldsymbol{\theta})$ as follows:

$$\dot{\boldsymbol{p}} = J(\boldsymbol{\theta})\dot{\boldsymbol{\theta}} \tag{57}$$

where

$$\boldsymbol{p} = \left[\, x_e\ y_e \,\right]^T \tag{58}$$

and

$$J(\boldsymbol{\theta}) = \begin{bmatrix} -L_0 \sin\theta_0 - L_1 \sin(\theta_0 + \theta_1) & -L_1 \sin(\theta_0 + \theta_1) \\ L_0 \cos\theta_0 + L_1 \cos(\theta_0 + \theta_1) & L_1 \cos(\theta_0 + \theta_1) \end{bmatrix} \tag{59}$$

6 Appendix 2: Calculation of control law

Using (9), $\dot{\boldsymbol{\theta}}_r$ becomes

$$\begin{aligned} \dot{\boldsymbol{\theta}}_r &= \dot{\boldsymbol{\theta}}_d + K_a(\boldsymbol{\theta}_d - \boldsymbol{\theta}) \\ &= \dot{\boldsymbol{\theta}}_d^* + \Delta\dot{\boldsymbol{\theta}}_d^* + K_a(\boldsymbol{\theta}_d^* + \Delta\boldsymbol{\theta}_d^* - \boldsymbol{\theta}) \\ &= \dot{\boldsymbol{\theta}}_r^* + \Delta\dot{\boldsymbol{\theta}}_r^* \end{aligned} \tag{60}$$

where

$$\Delta\dot{\boldsymbol{\theta}}_r^* = \Delta\dot{\boldsymbol{\theta}}_d^* + K_a\Delta\boldsymbol{\theta}_d^* \tag{61}$$

Assuming that all the dynamical parameters are known, the control law (3) can be rewritten as follows:

$$\begin{aligned} \boldsymbol{\tau} &= M(\boldsymbol{\theta})\ddot{\boldsymbol{\theta}}_r + C(\boldsymbol{\theta}, \dot{\boldsymbol{\theta}})\dot{\boldsymbol{\theta}}_r - K_d(\dot{\boldsymbol{\theta}} - \dot{\boldsymbol{\theta}}_r) \\ &= M(\boldsymbol{\theta})\ddot{\boldsymbol{\theta}}_r^* + C(\boldsymbol{\theta}, \dot{\boldsymbol{\theta}})\dot{\boldsymbol{\theta}}_r^* \\ &\quad + M(\boldsymbol{\theta})\Delta\ddot{\boldsymbol{\theta}}_r^* + (C(\boldsymbol{\theta}, \dot{\boldsymbol{\theta}}) + K_d)\Delta\dot{\boldsymbol{\theta}}_r^* \\ &\quad - K_d(\dot{\boldsymbol{\theta}} - \dot{\boldsymbol{\theta}}_r^*) \\ &= Y_L(\boldsymbol{\theta}, \dot{\boldsymbol{\theta}}, \dot{\boldsymbol{\theta}}_r^*, \ddot{\boldsymbol{\theta}}_r^*)\boldsymbol{\sigma}_L \\ &\quad + [M(\boldsymbol{\theta})\Delta\ddot{\boldsymbol{\theta}}_r^* + (C(\boldsymbol{\theta}, \dot{\boldsymbol{\theta}}) + K_d)\Delta\dot{\boldsymbol{\theta}}_r^*] \\ &\quad - K_d\boldsymbol{s} \end{aligned} \tag{62}$$

It can be seen from Eq. (61) that the second term in Eq. (62) is a function of $\Delta\boldsymbol{\theta}_d^*$, $\Delta\dot{\boldsymbol{\theta}}_d^*$, and $\Delta\ddot{\boldsymbol{\theta}}_d^*$. If we compare Eq. (10) with Eq. (62), the second term of (10) will be written as follows using (13)

$$\begin{aligned} &\boldsymbol{\tau}_\Delta(\Delta\boldsymbol{\theta}_d^*, \Delta\dot{\boldsymbol{\theta}}_d^*, \Delta\ddot{\boldsymbol{\theta}}_d^*) \\ &= [M(\boldsymbol{\theta})\Delta\ddot{\boldsymbol{\theta}}_r^* + (C(\boldsymbol{\theta}, \dot{\boldsymbol{\theta}}) + K_d)\Delta\dot{\boldsymbol{\theta}}_r^*] \\ &= M(\boldsymbol{\theta})(\Delta\ddot{\boldsymbol{\theta}}_d^* + K_a\Delta\dot{\boldsymbol{\theta}}_d^*) \\ &\quad + (C(\boldsymbol{\theta}, \dot{\boldsymbol{\theta}}) + K_d)(\Delta\dot{\boldsymbol{\theta}}_d^* + K_a\Delta\boldsymbol{\theta}_d^*) \\ &= M(\boldsymbol{\theta})\Delta\ddot{\boldsymbol{\theta}}_d^* + (M(\boldsymbol{\theta})K_a + C(\boldsymbol{\theta}, \dot{\boldsymbol{\theta}}) + K_d)\Delta\dot{\boldsymbol{\theta}}_d^* \\ &\quad + (C(\boldsymbol{\theta}, \dot{\boldsymbol{\theta}}) + K_d)K_a\Delta\boldsymbol{\theta}_d^* \\ &= M(\boldsymbol{\theta})\ddot{Y}_\phi(t)\boldsymbol{\sigma}_c + (M(\boldsymbol{\theta})K_a + C(\boldsymbol{\theta}, \dot{\boldsymbol{\theta}}) + K_d)\dot{Y}_\phi(t)\boldsymbol{\sigma}_c \\ &\quad + (C(\boldsymbol{\theta}, \dot{\boldsymbol{\theta}}) + K_d)K_a Y_\phi(t)\boldsymbol{\sigma}_c \\ &= Y_\psi(t)\boldsymbol{\sigma}_c \end{aligned} \tag{63}$$

where

$$\begin{aligned} Y_\psi(t) = M(\boldsymbol{\theta})\ddot{Y}_\phi(t) &+ (M(\boldsymbol{\theta})K_a + C(\boldsymbol{\theta}, \dot{\boldsymbol{\theta}}) + K_d)\dot{Y}_\phi(t) \\ &+ (C(\boldsymbol{\theta}, \dot{\boldsymbol{\theta}}) + K_d)K_a Y_\phi(t) \end{aligned} \tag{64}$$

This gives us Eq. (16).

7 Appendix 3: Boundedness

Based on assumption A7, $\boldsymbol{\theta}_d^*$, $\dot{\boldsymbol{\theta}}_d^*$, $\ddot{\boldsymbol{\theta}}_d^*$ are bounded. $Y_\psi(t)$ is also bounded as assumed in Theorem 1. Furthermore, $M(\boldsymbol{\theta})$ is bounded since each element contains only constants or cosine functions.

Because $\dot{V} \leq 0$, $V(0) \geq V > 0$, V is bounded, i.e., $\boldsymbol{s}$ and $\bar{\boldsymbol{\sigma}}_c$ are bounded. The boundedness $\boldsymbol{s}$ ensures the boundedness of $\dot{\boldsymbol{\theta}}$ and $\dot{\boldsymbol{\theta}}_r^*$. The boundedness of $\dot{\boldsymbol{\theta}}_r^*$ means that $\boldsymbol{\theta}$ is bounded (see Eq. (11)). Thus, $C(\boldsymbol{\theta}, \dot{\boldsymbol{\theta}})$ is also bounded.

We can ensure the boundedness of $\dot{\boldsymbol{s}}$ because of Eq. (23) and the nonsingularity of $M(\boldsymbol{\theta})$.

Because we can obtain the boundedness of $\boldsymbol{s}$ and $\dot{\boldsymbol{s}}$, $\ddot{V}$ given by (29) becomes bounded.

References

Aström K, Wittenmark B (1989) Adaptive control. Addison-Wesley, Boston

Bernier P, Burle B, Vidal F, Hasbroucq T, Blouin J (2009) Direct evidence for cortical suppression of somatosensory afferents during visuomotor adaptation. Cereb Cortex 19(9):2106–2113

Berret B, Chiovetto E, Nori F, Pozzo T (2011) Manifold reaching paradigm: how do we handle target redundancy? J Neurophysiol 106(4):2086–2102

Bhushan N, Shadmehr R (1999) Computational nature of human adaptive control during learning of reaching movements in force fields. Biol Cybern 81(1):39–60

Chien M-C, Huang A-C (2004) Adaptive impedance control of robot manipulators based on function approximation technique. Robotica 22(4):395–403

Darainy M, Mattar AAG, Ostry DJ (2009) Effects of human arm impedance on dynamics learning and generalization. J Neurophysiol 101(6):3158

Davidson P, Wolpert D (2004) Scaling down motor memories: de-adaptation after motor learning. Neurosci Lett 370(2):102–107

Flash T (1987) The control of hand equilibrium trajectories in multi-joint arm movements. Biol Cybern 57(4):257–274

Flash T, Hogan N (1985) The coordination of arm movements: an experimentally confirmed mathematical model. J Neurosci 5(7):1688

Galicki M (2007) Adaptive path-constrained control of a robotic manipulator in a task space. Robotica 25(1):103–112

Gomi H, Kawato M (1996) Equilibrium-point control hypothesis examined by measured arm stiffness during multijoint movement. Science 272(5258):117

Gribble PL, Ostry DJ, Sanguineti V, Laboissière R (1998) Are complex control signals required for human arm movement? J Neurophysiol 79(3):1409

Huang S, Tan K, Lee T (2008) Adaptive neural network algorithm for control design of rigid-link electrically driven robots. Neurocomputing 71(4–6):885–894

Ito S, Aoyama Y, Kawasaki H (2003) A static balance control under periodic external force. In: SICE 2003 annual conference, pp 600–605

Ito S, Kawasaki H (2005) Regularity in an environment produces an internal torque pattern for biped balance control. Biol Cybern 92(4):241–251

Izawa J, Rane T, Donchin O, Shadmehr R (2008) Motor adaptation as a process of reoptimization. J Neurosci 28(11):2883–2891

Kambara H, Kim K, Shin D, Sato M, Koike Y (2009) Learning and generation of goal-directed arm reaching from scratch. Neural Netw 22(4):348–361

Katayama M, Kawato M (1993) Virtual trajectory and stiffness ellipse during multijoint arm movement predicted by neural inverse models. Biol Cybern 69(5):353–362

Kistemaker DA, Soest AKJV, Bobbert MF (2007) Equilibrium point control cannot be refuted by experimental reconstruction of equilibrium point trajectories. J Neurophysiol 98(3):1075

Malfait N, Shiller D, Ostry D (2002) Transfer of motor learning across arm configurations. J Neurosci 22(22):9656–9660

Massone L, Bizzi E (1989) A neural network model for limb trajectory formation. Biol Cybern 61(6):417–425

Mitrovic D, Klanke S, Vijayakumar S (2011) Learning impedance control of antagonistic systems based on stochastic optimization principles. Int J Robotics Res 30(5):556

Miyamoto H, Kawato M, Setoyama T, Suzuki R (1988) Feedback-error-learning neural network for trajectory control of a robotic manipulator. Neural Netw 1(3):251–265

Mussa-Ivaldi F, Hogan N, Bizzi E (1985) Neural, mechanical, and geometric factors subserving arm posture in humans. J Neurosci 5(10):2732–2743

Nguyen-Tuong D, Peters J (2011) Model learning for robot control: a survey. Cogn Process 12(4):319–340

Ostry DJ, Darainy M, Mattar AAG, Wong J, Gribble P (2010) Somatosensory plasticity and motor learning. J Neurosci 30(15):5384

Shadmehr R, Mussa-Ivaldi FA (1994) Adaptive representation of dynamics during learning of a motor task. J Neurosci 14(5):3208

Slotine J-JE, Li W (1987) On the adaptive control of robot manipulators. Int J Robotics Res 6(3):49

Slotine J-JE, Li W (1991) Applied nonlinear control, vol 66. Prentice hall, Englewood Cliffs

Sutton R, Barto A (1998) Reinforcement learning: an introduction, vol 116. Cambridge University Press, Cambridge

Tee KP, Franklin DW, Kawato M, Milner TE, Burdet E (2010) Concurrent adaptation of force and impedance in the redundant muscle system. Biol Cybern 102(1):31–44

Todorov E, Jordan MI (2002) Optimal feedback control as a theory of motor coordination. Nat Neurosci 5(11):1226–1235

Todorov E, Jordan MI (1998) Smoothness maximization along a predefined path accurately predicts the speed profiles of complex arm movements. J Neurophysiol 80(2):696

Tsuji T, Morasso PG, Goto K, Ito K (1995) Human hand impedance characteristics during maintained posture. Biol Cybern 72(6):475–485

Uno Y, Kawato M, Suzuki R (1989) Formation and control of optimal trajectory in human multijoint arm movement. Biol Cybern 61(2):89–101

Wolpert DM, Ghahramani Z, Jordan MI (1995) An internal model for sensorimotor integration. Science 269(5232):1880